Conor J. Walsh
Massachusetts Institute of Technology,
Department of Mechanical Engineering,
Cambridge, MA 02139;
Massachusetts General Hospital,
Department of Radiology,
Boston, MA 02114

Arjan J. H. Meskers
Technical University of Delft,
Department of Biomedical Engineering,
Delft, 2600 AA, The Netherlands

Alexander H. Slocum
Massachusetts Institute of Technology,
Department of Mechanical Engineering,
Cambridge, MA 02139

Rajiv Gupta
Massachusetts General Hospital,
Department of Radiology,
Boston, MA 02114

CT-Compatible Medical Drilling Stylet

This paper describes the design of a compact, lightweight CT-compatible, drill-press that is designed to be used in either a hand-held or stand-alone mode to assist with percutaneous bone based interventions. Previous medical drilling tools that have been developed have a metal structure and typically have one actuator for advancing the drill (feed) and another for rotating it (speed). After defining the device functional requirements and specifications, a deterministic design process was followed to generate several design concepts that were then evaluated based on their ability to satisfy the functional requirements. A final concept that uses a custom screw-spline to achieve helical motion of a shaft that is attached to a standard orthopedic drill was selected for prototyping. The design uses a single actuator to drive both the screw and spline nuts through two different gear ratios, resulting in a fixed ratio between the feed and speed. Apart from the motor which is placed away from the central drill axis, the device is largely made from plastic materials. A custom experimental setup was developed that enabled drilling into bone inside a CT scanner to be examined. Results showed that the device was successfully able to penetrate thick cortical bone and that its structure did not appreciably distort the medical images. [DOI: 10.1115/1.4007280]

Keywords: medical robotics, computed tomography, X-ray, drill, interventional radiology, bone

1 Introduction

Minimally invasive, image-guided interventional radiological procedures typically entail insertion of an instrument through a small incision and its subsequent dexterous manipulation while viewing fluoroscopic, computed tomography (CT), ultrasound, or magnetic resonance (MR) images. These procedures are gradually replacing more invasive or open surgical procedures, resulting in reduced trauma and recovery time for patients. With the development of new miniaturized diagnostic and treatment tools the number of procedures performed in this manner is continuing to grow. Further, new portable imaging devices (e.g., CereTom, Neurologica, Danvers, MA) mean that physicians will soon have easy access to high resolution images in the operating room and the time and logistical challenges associated with imaging will be reduced.

In musculoskeletal radiology [1], bone biopsy or ablation are common procedures performed for the diagnosis and treatment of disease. For example, the most common treatment of an osteoid osteoma, a small benign lesion that is most frequently found in the leg [2,3], is by image-guided radio frequency ablation of its nidus. For these procedures, a coaxial needle system is typically used, where the outside cannula is placed at the bone surface after which an inner cutting stylet is advanced through the bone. When the cortical bone is thin, it can typically be punctured by applying direct manual pressure to a sharp needle. However, when it is thicker, the needle is typically "tapped" using a surgical hammer. These approaches require significant effort from a physician and provide poor control over needle entry into bone and may result in over-shooting the lesion when the stylet breaks through the stiff cortical surface. Once the target is reached, the stylet is removed and ideally the cannula should stay in place so as to provide an access pathway through the cortical bone. If the cannula is to move (e.g., due to table movement or respiration), its realignment can be difficult. To address this, a drilling stylet that creates a hole of larger diameter than the concentric outer cannula is often used so that the cannula can then be anchored in the hole created in the cortical bone [4]. Apart from bone biopsy and ablation, there are many other procedures that involve percutaneous insertion of tools into bone, e.g., vertebro- and kyphoplasty for vertebral augmentation, transpedicular screw placement for posterior spinal fixation, drainage of deep bone abscesses, and many other neurosurgical procedures.

One example neurosurgical application is for precisely accessing various structures inside the body such as the petrous apex or the cochlea in the temporal bone in a minimally invasive manner. The advent of ultrahigh resolution CT scanners, for example, flat-panel scanners [5], has enabled the key anatomy to be visualized noninvasively; thus opening up the possibility of image-guided interventions. One such procedure that can now be performed under image-guidance is that of cochlear implantation where an electrode is passed through the mastoid cavity and into the cochlea [6]. With this approach, accuracy is of paramount importance as any deviation of the drill from the desired trajectory can lead to damage of the facial nerve and chorda tympani. Thus, it is highly desirable to be able to simultaneously advance a drill bit and image to ensure a safe trajectory is maintained.

Thus, from a clinical point of view, a medical drill for percutaneous interventions should be

1. Compatible with X-ray or CT imaging.
2. Able to controllably advance the drill to the desired depth.
3. Modular, so it can be used in hand-held mode or mounted to a stereotactic frame.
4. Minimally complex, so that it can be lightweight and cost-effective.

1.1 Prior Art. To improve the ability of a physician to precisely penetrate bone, many different strategies have been proposed for automating the drilling operation or providing some means of drill alignment or tracking. Buckley et al. coupled the hub of a needle to a drill and found that this provided a cheap, safe, and efficient technique for reducing physician effort for obtaining core biopsy samples [7]. Onogi et al. employed a mechanism to rotate a standard percutaneous needle in a reciprocating

Manuscript received March 8, 2010; final manuscript received April 10, 2011; published online October 11, 2012. Assoc. Editor: Paul A. Iaizzo.

manner during insertion and found that a force of 25 N was required when the feed rate of the needle was 0.05–0.5 mm/s [8]. The needle holder was guided by a stiff supporting robot arm that resisted the insertion forces. For percutaneous cochlear implantation a drill was attached to an industrial robot whose position was monitored with an image-based tracking system and in 9 out of 10 cases, the drill bit successfully accessed the basal turn of the cochlea without damage to the facial nerve [9]. Guidance was achieved via a fiducial-based registration and the drilling was performed by a physician while they watched a virtual model of the anatomy and advancing drill [6]. The researchers reported that maintaining the drill along its desired path was difficult and thus to improve accuracy, they developed small patient-specific stereotactic frames [10] that incorporated a drill guide. Each frame was attached to anchors mounted in the bone that also acted as fiducial markers for achieving submillimeter registration accuracy between the drill guide and prior head CT. In an initial in vivo study they successfully guided the drill through the facial recess in 5 out of 5 cases without injury to the facial nerve [11]. However, for the above procedures there was no visualization of the actual drill bit as it was advancing inside the skull.

Other systems to position a drill mounted on an automated feeding device have been developed for spinal fusion [12] and neurosurgical [13] procedures. For each of these systems the drilling portion consists of one actuator for rotating the drill that is mounted on a carriage driven by another actuator. The drilling system mentioned in [13] is described in detail in [14] and consists of a large metallic structure. It is equipped with a control system that monitors current drawn by the motors in order to detect when the drill passes through different layers of bone tissue. Another device from Kopf industries (US 5|370|481) combines a drill with a manually actuated carriage (i.e., a drill press) that can be used in conjunction with a stereotactic frame. The advancement of the drill is decoupled from the orientation of the tool with the stereotactic frame providing a sufficiently stiff support structure when locked in place.

The aforementioned drilling systems are all constructed with metal parts and are thus heavy and not designed to be used in conjunction with medical imaging systems. Recognizing this fact, Cole et al. [15] designed an X-ray transparent drill *adapter* for use in orthopedic procedures (US 5,013,317). The device consists of a right-angle gearbox that is constructed from plastic components so than the drill can be out of the line of sight of the drill bit when the surgeon is aligning the drill with a trajectory visualized via the X-ray field. Although this enables clear visualization of drilling under image-guidance, drilling is still performed manually and the surgeon has no means to advance the drill automatically or precisely control the depth of drilling.

1.2 Contribution. In this paper we outline the design of a CT-compatible medical drilling stylet for percutaneous interventions that can provide rotation and axial feeding of any standard medical drill bit or bone cutting tool. The device is based on the concept of a screw-spline and provides a metal free scan plane to not distort the CT images. The device mates with standard access cannulas to protect soft-tissue from the drilling action and provide an access path to the desired target after drilling is complete. This modular "drill press" can easily mount to existing positioning and alignment systems for use during intra-operative imaging or could be operated in a hand-held mode by a radiologist as part of standard image-guided procedure protocols.

2 Defining Device Specifications

The primary goal of this project was to create a CT-compatible drill-press that should be capable of translating and rotating the drill bit while used in stand-alone or manual mode. A deterministic design process was taken with a first step of understanding the various aspects on the challenge to develop quantitative specifications for the device.

2.1 Drilling Parameters for Bone. Drilling into bone is a commonly performed surgical intervention, however there has been limited research attention on the parameters (thrust, torque, feed, and speed) required to drill into bone. To complicate matters further, there is a large amount of variation in the hardness of different bones; it is affected by its mineral density, anatomic site, person age, race, and gender. This leads to wide variation in the drilling parameters required for a particular drilling operation. Furthermore, the size and cutting geometry of the drill bit has also been shown to affect the forces and torques required for drilling into bone [16]. Hillery and Shuaib measured the force and torque required for drilling into bone with a 3.2 mm diameter drill by rigidly fixing a sample of bone to a dynamometer [17]. For these experiments the drill point and rake angles were 70 deg and 23 deg, respectively, and a feed rate of 50 mm/min was used. They found a max torque of 14.5 N mm at 400 rpm that decayed to 1.5 N mm at 2000 rpm. They found a corresponding decrease in the force, 48 N at 400 rpm to 23 N at 2000 rpm. They also found that as a drill-bit traveled further into the bone there was an increase in temperature due to the inability of the bone to conduct generated heat away from the drilling site. In general it is desirable to not have a large rise in temperature during drilling as it has been shown that if bone is exposed for 30 s at 50 °C then cellular necrosis will be induced [18]. A study by Ohashi et al. showed that a reduced thermal damage to bone when drilling at speeds of 200 and 500 rpm compared to 5000 rpm, though the slower speeds introduced a lower degree of circularity for the hole [19].

2.2 CT-Compatible Structure. CT-images are based upon X-ray emission from the scanner, which originates from electrons impacting a metal cathode, with the absorption of this emitted radiation giving an indication of the material density. For medical computed tomography, materials with a higher density than bone (e.g., metals) will lead to streaking artifacts. This occurs because the density of the material is beyond the expected range for medical applications [20]. The thin tubular tools used by physicians do appear brightly in the medical images but only create minimal artifacts as the volume of metal is sufficiently low. Thus, any drilling device should not introduce any additional metal into the CT images adjacent to the medical instrument being used, i.e., the drill.

2.3 Access to Bone Through Tissue. In any medical drilling procedure the drill has to access bone through soft-tissue whose thickness will depend of the anatomic location of the bone as illustrated in Fig. 1. As such, any drilling device should provide some means to protect the tissue from the rotating drill bit and provide an access path through the soft tissue.

Drilling a hole under a nonorthogonal position into bone will result in wandering of the drill bit along the surface of the bone before it creates a hole that acts to constrain further motion. The severity of this wandering motion will depend on the angle of approach, axial force applied, rotational speed of the drill, the shape of the drill bit and how the driven end of the drill bit is constrained. For the case that the proximal end of the drill is rigidly constrained, this will lead to bending and even breaking of the drill bit. Thus it is necessary to prevent the drill from wandering so as to ensure accurate and safe drilling.

2.4 Device Mounting and Support. Any drilling device will need to counter the reaction forces created when drilling. This can be applied manually by a physician holding the device or a sufficiently stiff support structure that can be mounted on or next to the patient as illustrated in Fig. 2.

3 Device Design: Concept Selection

The first step in the deterministic design process was to establish quantitative and qualitative functional requirements for the device from the design specifications outlined in Sec. 2 (Table 1).

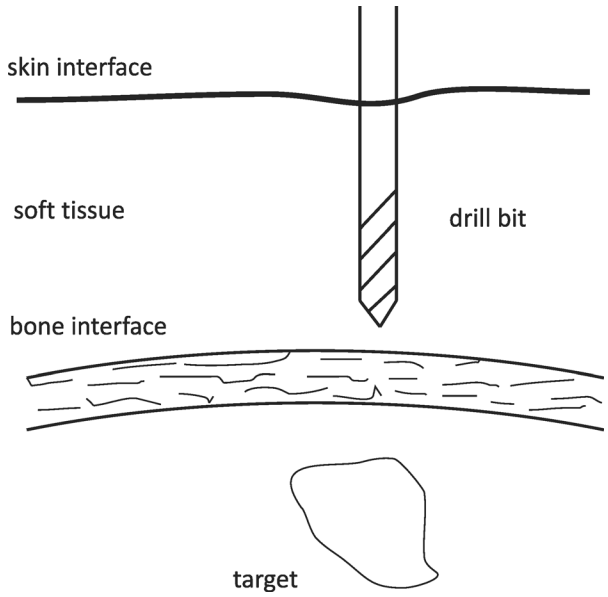

Fig. 1 Illustration of a drill about to penetrate a layer of bone. During the drilling operation there should be a means to protect the soft-tissue from the drilling action. After an access path through the bone has been created, there should be some means to access this from the skin surface.

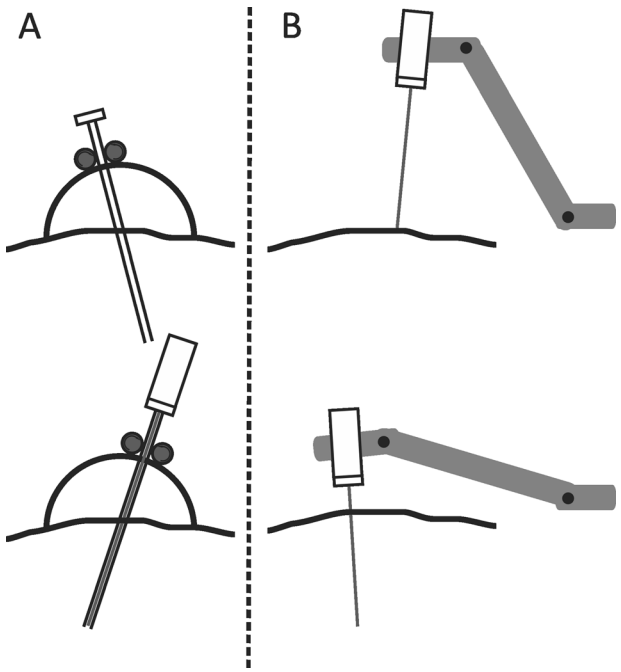

Fig. 2 Possible methods for supporting the drilling stylet. In A, the stylet could be attached to a standard cannula that is first placed to the desired bone entry site. In B, the drilling stylet could be mounted on the end of an active or passive positioning arm.

The key focus of the design process was on developing a compact and lightweight mechanism that could meet the functional requirements listed while minimizing cost and maximizing safety. Based on this, we developed three drive mechanism concepts that could achieve this.

3.1 Concept 1: Linear Carriage and Motor. One method to implement automated drilling would be to have one motor for rotating the drill shaft that would be mounted on a linear carriage driven by a second motor with a leadscrew as shown in Fig. 3. A variant of the first linear carriage concept has been previously used in medical drilling procedures [14], although it was bulky and not CT-compatible. By varying the speed of both motors a range of feeds and speeds can be achieved. For this concept, the drive mechanism for rotating the drill, as well as its support structure, has to be advanced by the motor that drives the leadscrew. This device could be made CT-compatible by making all of the parts (apart from the motors) out of plastics and positioning of the motors in such a way as to provide a metallic free scan plane in a manner similar to [20]. However, this concept involves moving the mass of the motor and the transmission force of the leadscrew is not in line with the drill which may lead to binding of the carriage with the linear guide rods due to off-axis loading.

Table 1 Device functional requirements

1	Provide at least 50 N of thrust force and 0.5 Nm of torque
2	Feed-rate range of 0.1–0.5 mm/s
3	Drill rotational speed range of 100–500 rpm
4	Metallic free scan plane to minimize device artifact
5	Have a maximum device diameter of 70 mm
6	Protect the soft-tissue from damage during drilling
7	Provide access to the desired site after the drilling operation
8	Used in hand-held or stand-alone mode

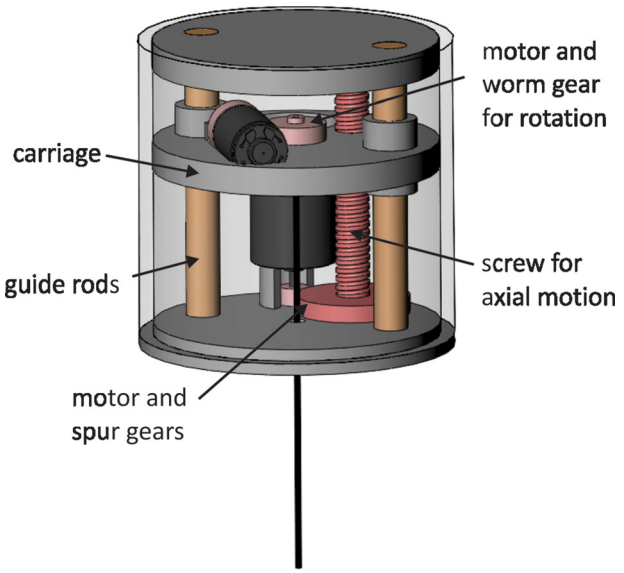

Fig. 3 Concept 1. A motor is used to drive the drill rotation that moves on a carriage that is driven using a motor and leadscrew. In this concept, independent control of the drilling feed and speed can be controlled.

A first order analysis was performed to determine if such a transmission could provide the necessary force and torque in a compact package. For a linear power screw, the total shaft torque required is a function of the required force, F, pitch diameter, d_m, lead, l, and coefficient of friction μ and the thread angle, α. Thus, neglecting frictional forces arising from bearings, the general equation for calculating the torque to raise a load is

$$T = \frac{Fd_m}{2}\left(\frac{l + \pi\mu d_m \sec\alpha}{\pi d_m - \mu l \sec\alpha}\right) \quad (1)$$

If T_0 is the achievable torque assuming no frictional losses due to sliding contact between the threads, the efficiency, e, for power transmission with a screw is given by

$$e = \frac{T_0}{T} = \frac{Fl}{2\pi T} \tag{2}$$

Another important consideration when sizing a power screw transmission is the maximum stress it will experience. The equivalent von Mises stress at the root diameter of the screw, d_r, is calculated by combining the axial and shear stresses

$$\sigma_{\text{equivalent}} = 2^* \sqrt{\left(\frac{4F}{\pi(d_r)^2}\right)^2 + 3\left(\frac{16T}{\pi d_r^3}\right)^2} \tag{3}$$

Thus for the required axial force of 50 N, a typical coefficient of friction for plastic sliding on plastic of 0.2, a pitch diameter of 10 mm, a lead of 1.5 mm and a thread angle of 29 deg, we find that the required torque for the screw is 61 N mm which would be achievable with a small motor and transmission. Based on this input torque and output axial force, the maximum equivalent von Mises stress in the screw shaft is 2.5 MPa, which is well below the maximum allowable stress of 58 MPa for Acetal. This preliminary analysis shows that it is feasible to make such a power screw of reasonable size out of plastic with an approximate screw efficiency of 20%.

3.2 Concept 2: Angled Traction Drive. This concept was inspired by the Roh'Lix actuator (Zero-Max Inc., Plymouth, MN, USA). It is a drive mechanism that is designed to convert rotary motion into linear motion using rollers mounted at an angle relative to a drive shaft as illustrated in Fig. 4. The normal force between the rollers and the drive shaft, F_n, and coefficient of friction, μ, between the parts determines the maximum torque and axial force that can be generated. The lead, l, is a function of the diameter of the drive shaft, d, and the angle between it and the drive roller, which for a given lead is calculated from

$$\tan\phi = \frac{l}{\pi d} \tag{4}$$

For this concept, helical motion of a tool could be achieved by replacing one (or more) of the free spinning rollers with an angled traction drive roller. A first order analysis was performed to see if making such a drive mechanism from plastic was feasible. For a desired axial force, the required shaft torque is given by

$$\tau = \frac{Fl}{\eta 2\pi} \tag{5}$$

where the efficiency, η, of the mechanism, is approximately 90% because power is transmitted via rolling motion. For two crossed cylinders, with an angle, φ, between their axes, an exact solution for the Hertz contact stress can be calculated [21]. Furthermore, for traction drives where the bodies are also in rolling contact, there will be local contact stresses resulting from the tangential drive force. The tangential stress can be estimated by the tangential force divided by the contact area, A. The maximum shear stress can then be approximated as the sum of the Hertz and tangential stress components. Using the methodology outlined in [21] the maximum shear stress at the contact interface between the two rollers for some realistic dimensions was determined.

A 4.5 mm lead and a 6 mm main shaft diameter results in a mounting angle of 13.5 deg. To achieve an axial force of 50 N a torque of 36 N mm would be required. The lead was chosen to be large, 4.5 mm, in order to achieve sufficient shaft torque for drilling into bone. Thus a larger lead could be used with a larger motor or a motor and transmission. From the Hertz contact analysis (see spreadsheet in Appendix), the maximum shear stress between the rollers was 14.7 MPa which is about one quarter of the allowable value for Acetal. Thus, this first order analysis demonstrated that it is feasible to construct an appropriately sized CT-compatible drilling device using an angled roller concept to generate the necessary helical motion. This concept requires only a single motor to generate helical drilling motion, although a fixed ratio between the rotational speed and feed-rate is a consequence of such an approach. This design also has very efficient power transfer and has the drilling force concentric with the main shaft. Further, the shaft is the only part of the device that has to move with the rest of the support structure remaining stationary. However, there is a risk of slipping of the main shaft due to a friction based means of actuation.

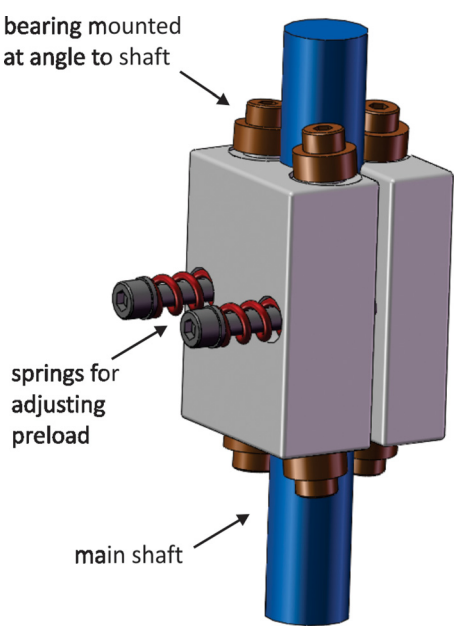

Fig. 4 Concept 2. An angled traction drive, where the rollers are not mounted parallel to an inserted shaft (source-file: modified www.zero-max.com solid works file).

3.3 Concept 3: Screw-Spline. The final concept explored for generating helical motion in a compact package was a screw-spline. A screw-spline consists of a threaded screw that also has a splined groove along its length. It is functionally similar to the ball-screw spline that is produced by THK that has been used in SCARA robots (e.g., EPSON RS3-Series, EPSON Robots, CA 90 746) and other robotic applications where the combination of translation and rotation are required in a compact design [22]. Figure 5 shows a section view of a screw-spline mechanism that is driven through a set of spur gears by two dc motors that was developed for another application in our laboratory.

The spline and screw nuts are driven by the two motors and engage the spline and threads of the shaft, respectively. By varying the speed of the two motors a wide range of feeds and speeds can be achieved. A clear metallic free zone can also be achieved whose size depends only on the diameter of the gears that are used to mate with the motor shafts. It would also be possible to use remote actuation with this device to make it fully CT compatible. From the first order analysis of concept 1 we showed that making a plastic screw of 10 mm in diameter that can handle the necessary forces and torques is feasible. The resultant motion of the screw-spline will be a function of the rotation of both the screw and spline nuts. The rotational speed of the screw-spline is simply the rotational speed of the spline nut, ω_1. The feed rate, v, of the drilling device is a function of, ω_1, and also the rotational speed of the screw nut, ω_2,

$$v = \frac{l}{2\pi}(\omega_1 - \omega_2) \tag{6}$$

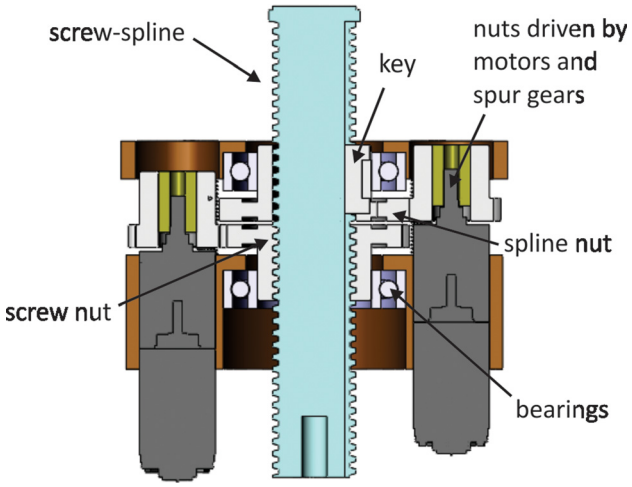

Fig. 5 Concept 3. A screw-spline used to control the drilling feed and speed. It consists of a plastic threaded rod that also has a spline along it. Motors are connected to a threaded and keyed nut that engage the screw and spline, respectively.

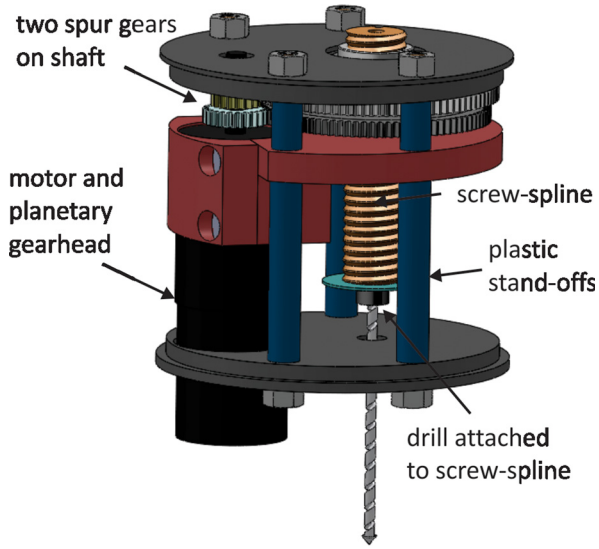

Fig. 6 Final design of the single motor driven screw-spline mechanism with a single motor driving the screw and spline nuts through different gear ratios

Table 2 Pugh chart for concept selection

	Concept 1	Concept 2	Concept 3
Minimal moving mass	(−)	(+)	(+)
CT transparent zone	0	0	0
Minimal support structure	0	(+)	(+)
Drive force concentric with drill	(−)	(+)	(+)
Efficiency	(−)	(+)	(−)
Nonbackdrivability	(+)	(−)	(+)
Risk of slip	(+)	(−)	(+)
Total	**−1**	**2**	**4**

It can be seen that if the speeds of these nuts are equal then the shaft will only rotate and not translate. Similar to concept 2, the screw-spline concept has a much smaller moving mass compared to concept 1. This concept also provides a very efficient means of obtaining a metallic free zone. As was shown in Fig. 5, a screw-spline typically has two motors for actuating the screw and spline nuts independently. Inspired by the single motor "angled traction-drive" concept, a variant on the screw-spline concept was one where both nuts were driven off the same motor shaft, but with different transmission ratios.

3.4 Concept Assessment. With this modified concept 3, a Pugh chart was created (Table 2) to help select a concept to prototype. As can be seen, the single-motor screw-spline, concept 3, was deemed the most promising choice for prototyping with the linear carriage design being the least favorable. The angled traction drive, concept 2, had many positives but the risk of slipping and the ability to back-drive were the main reasons that it was not pursued. However, the previously described first order analysis showed that it is feasible to create such a mechanism out of plastic.

4 Device Design: Mechanism Design and Manufacturing

The final CAD model of the device is shown in Fig. 6. It is designed from largely plastic components to be lightweight and largely radiolucent.

The linear travel of the device is determined by the length of the screw-spline shaft and the spacing of the nuts. For the design shown the linear travel is 30 mm and when the drill is initially fully retracted, the screw-spline shaft protrudes 30 mm above the top plate. The motor is located off the working axis of the drill bit, via the large diameter plastic spur gears of the nuts, creating a metallic free zone so as to not distort the medical images. The midplate has a mounting block for clamping the motor and gearhead. A bottom plate is offset from the mid plate with spacers and threaded rods and provides an attachment point for a standard medical cannula via a medical luer-lock. Assuming that the distal end of the cannula will be pressed superficially into bone, having the drill bit tip inside it decreases the chance of wandering. After the drill bit has advanced through the bone to the desired depth, the luer-lock can be used to remove the device, leaving the access cannula in place for sampling of tissue or injection of therapeutic agents. The modular nature of the device means that it can be used in conjunction with different gross positioning systems such as stereotactic frames or medical robots (e.g., for drilling into the temporal bone) and can be used in hand-held mode during an interventional procedure by a radiologist (e.g., for drilling to a precise depth during musculoskeletal or spinal interventions).

4.1 Actuation and Transmission. To simplify the control for the device, a stepper motor was chosen to drive the screw and spline nuts. A stepper motor with a stall torque of 20 N mm was selected with a 14:1 reduction planetary gearbox. To achieve translation of the drill bit, the screw and spline nuts are required to spin at different speeds. This was achieved through a different gear ratio between the spur gears on the gearbox shaft and the spur gears integral to the nuts. The screw and spline nut pitch diameters were chosen to be 48 mm (96 teeth) and 45 mm (90 teeth), respectively. The pitch diameter of the gears to engage the screw and spline nuts were 9 (18 teeth) mm and 12 mm (24 teeth), respectively, resulting in gear reductions of 5.33 and 3.75, respectively. The screw-spline has a pitch diameter of 11.1 mm and a lead of 1.75 mm and was supported by the screw and spline nuts.

The drilling speed and feed are thus a function of the motor speed, the gear reduction between the motor shaft and the nuts and the lead of the screw. The torque output can be determined in a similar manner with the force obtained from Eq. (1). Further, assuming that the stepper does not skip steps, the drill can be advanced to a desired depth by commanding a desired number of rotations.

4.2 Prototype Manufacturing. In order to validate the capability of the drilling mechanism, a prototype was manufactured that is shown in Fig. 7. The three plates and motor clamp were all machined out of Acetal. Nylon M12 threaded rod was cut to length and a 1.4 mm wide groove was milled along its length. The outer races of 24 mm OD Ceramic bearings (VXB) were glued into the top and mid plates. The screw and spline nuts were modified hubbed Acetal gears (SDP-SI) and were glued into the inner 15 mm bearings races. The hub of the screw gear was tapped to match the threads on the Nylon rod. A sleeve was machined into the hub of the spline gear with a broaching tool and a small key coupled the rotation of the nut and screw-spline shaft. The axial movement of the key relative to the spline gear was restricted by means of a pin on the key which fits a hole in the hub. The top and mid plates held the bearings that were separated by spacers to provide clearance between the two different diameter hubbed gears that spin in them. A 22 mm diameter bipolar stepper motor from (Faulhaber 2224 AM) engaged the 14:1 metal planetary gearbox (Faulhaber, 23/1). For the gearhead shaft, brass (screw) and steel (spline) spur gears were attached via shaft locker (Loctite 680). The distal end of the screw-spline shaft had a threaded hole for attaching the drill bit via a modified steel hex screw that was glued to the proximal end of a 1.7 mm diameter drill bit (OrthoMed, Portland, OR, USA) that was 127 mm long. A threaded hole in the bottom-plate was used to attach a female luer-lock for enabling connection with standard medical cannulas.

The drive electronics for the system were placed in a control box that would be located away from the patient on the CT bed. It was designed to be plugged into a standard 120 V wall outlet and connected via a USB cable to a laptop. Inside the box were off-the-shelf components; a USB stepper motor controller (PMX-4CX-SA, ARCUS Technology Inc., CA, USA), power supply (S-100 F, Astrodyne, MA, USA), and four stepper motor drivers (RD-021M8, RORZE, CA, USA).

5 Device Validation and Testing

A clinically realistic experiment was performed to determine if the device was capable of drilling into bone.

5.1 CT Compatible Test Rig. A custom CT-compatible test rig was constructed that allowed the device to be securely mounted above a specimen of bone inside a CT scanner. The setup is shown in Fig. 8. It consists of two plastic plates that are offset by 20 cm by four aluminum posts. Only the drilling device was scanned and so the only parts of the test rig in the CT images were the two plastic plates. Thus, there was no artifact generation from the test rig in the CT images. A pattern in the top plastic plate provided mounting points for the drilling device and a path for the drill. A bovine bone is shown fixed to the base plate.

5.2 Preliminary Results. Two CT scans of the device, one before and a second after drilling, are shown in Fig. 9 below. Before drilling, the screw-spline is almost in its highest position with the distal tip of the drill about 3 mm from the distal tip of the cannula. The cross-sectional image of the bone highlights the dense cortical shell surrounding the less dense cancelous bone and marrow. A shadowing artifact created by the needle makes it appear that a hole has already been drilled through the bone but this is not the case. Overall, by placing the motor out of the plane of the drill, it is apparent that minimal artifact is generated by the device. The only significant artifact comes from the M4 hex nut that was used to attach the drill shaft to the screw-spline. Using the custom interface, the device was commanded to drill to a depth of 25 mm with a feed of 0.43 mm/s and a rotational speed of 60 rpm.

The result is shown in Fig. 9. It is clear that the drill penetrated the dense cortical bone and is now located close to the center of

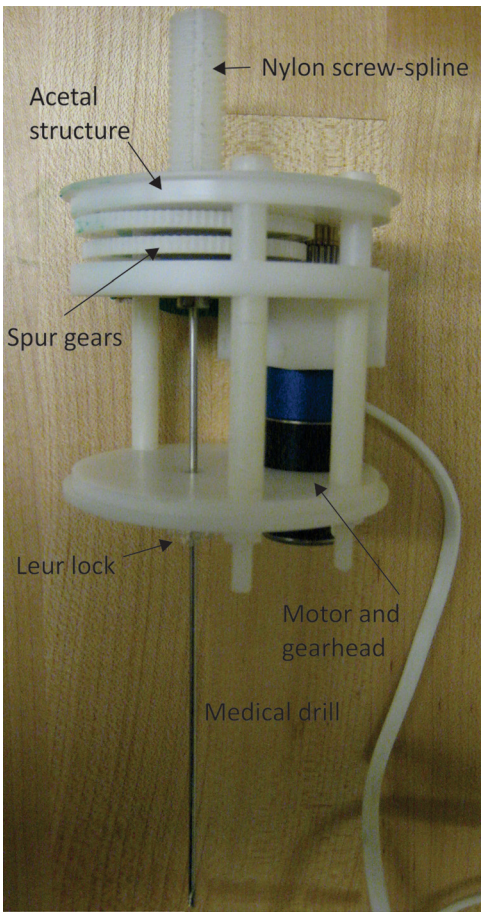

Fig. 7 Final prototype manufactured from largely plastic components. The motor is offset from the central axis of the drill.

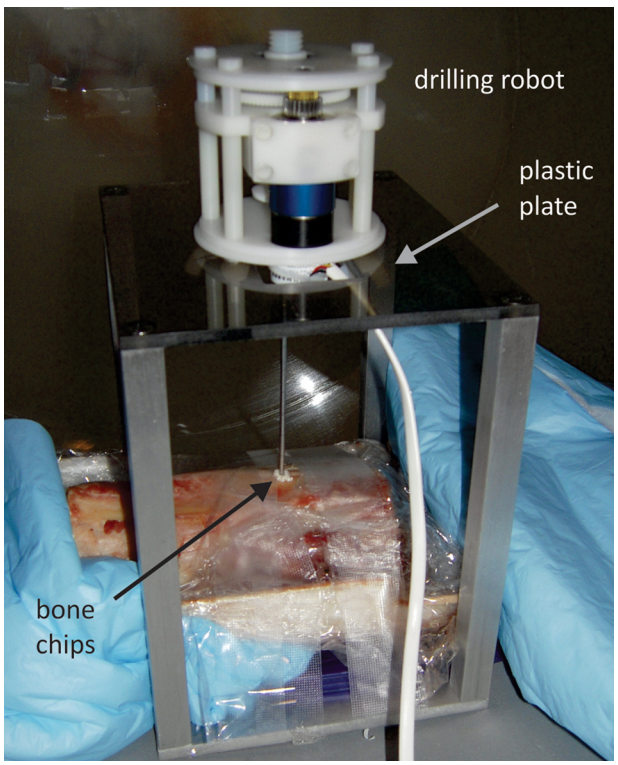

Fig. 8 CT-compatible test rig for supporting the device and a sample of bone

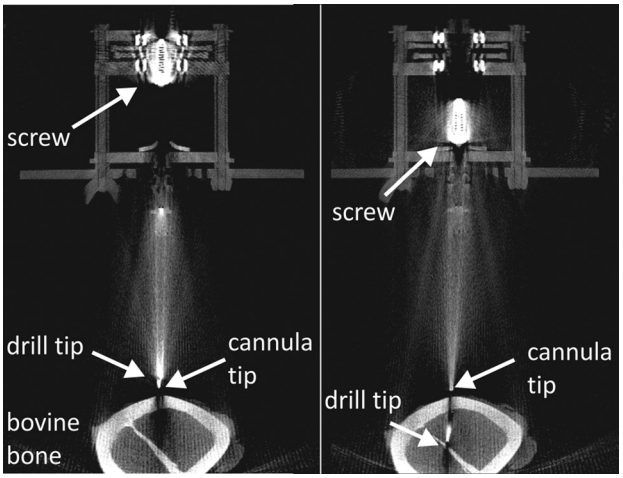

Fig. 9 CT scan of the device before and after drilling into the bovine bone. There is minimal streaking artifact from the device and the cannula and drill are clearly visible. While, the device was able to successfully drill into bone, some deflection of the bit was observed due to a small shift in the specimen.

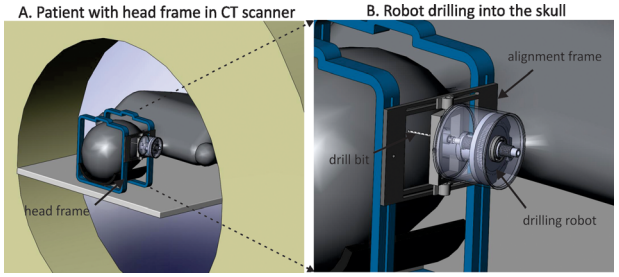

Fig. 10 Conceptual illustration of the CT-compatible drill press mounted on to a stereotactic frame for neurosurgical applications

the specimen of bone. Also, the hex nut threaded onto the base of the screw-spline can also be seen to have moved down by the same amount. Close inspection of the image reveals that the bone sample did shift slightly due to the forces during drilling. This is likely because the bone sample was not sufficiently secured to the test rig. However, it also highlights the challenge of preventing deflection of the drill bit and cannula due to the drill wanting to "walk." Thus there would be an advantage to first securing the cannula to the bone surface before beginning the drilling operation. This could be achieved by pressing the sharp cannula tip up against the bone surface and then giving it a gentle tap.

6 Conclusions and Future Work

Using a deterministic design process, several concepts for the device were generated and all the concepts were evaluated as to how they met the functional requirements. A final concept that uses a custom screw-spline to achieve helical motion of a shaft that is attached to a standard orthopedic drill was selected for α-prototyping. The design used a single actuator to drive both the screw and spline nuts through two slightly different gear ratios, resulting in a fixed ratio between the feed and speed. Apart from the motor which was placed away from the central drill axis, the device was largely made from plastic materials so as to not substantially distort the medical images. There was some distortion from the hex bolt used to secure the drill to the shaft but a less dense material for the attachment would greatly diminish this artifact. A preliminary experiment demonstrated that the device was capable of successfully drilling into bone.

Now that the use of a plastic screw-spline driven with a single motor has been validated, future work can focus on incorporating the CT-compatible drill press into an existing robot arm or a head mounted frame such as that shown in Fig. 10. Future experiments could evaluate the use of the device in realistic clinical procedures such as drilling precisely into a cadaver temporal bone while simultaneously imaging. Further, the effect of different gear ratios for the screw and spline nuts on the drilling process could be analyzed to find the optimal parameters for drilling into bone.

Acknowledgment

The authors would like to express their sincere appreciation to Dr. Daniel Rosenthal and Dr. Miriam Bredella for their valuable discussion on image-guided musculoskeletal interventions and the current tools that are available.

Appendix: The Spreadsheet That was Used to Implement the Equations Outlined in [21]

	A	B
1	**Hertz_Point_Contact.xls**	
2	To determine Hertz contact stress between bodies	
3	By Alex Slocum	
4	Enters numbers in BOLD, results in RED	
5	Lead (mm)	**4.5**
6	Lead angle (deg) (angle between rollers)	13.440
7	Desired axial force (N)	**50**
8	Coefficient of friction	**0.2**
9	Ronemaj (mm)	**1000000.000**
10	Ronemin (mm)	**3.000**
11	Rtwomaj (mm)	**1000000.000**
12	Rtwomin (mm)	**10.000**
13	Ultimate tensile stress (N/mm^2)	**69**
14	Elastic modulus Eone	**2.00 E + 03**
15	Elastic modulus Etwo	**2.00 E + 03**
16	Poisson's ratio vone	**0.34**
17	Poisson's ratio vtwo	**0.34**
18	Costheta	0.981
19	Theta	0.197
20	Alpha	6.011
21	Beta	0.324
22	Lambda	0.341
23	Shaft torque required (N mm)	35.828
24	Tangential force on shaft (N)	11.943
25	Preload force required (N)	59.713
26	Applied load F (N)	59.713
27	Phi (deg) (l90 is crossed rollers)	13.440
28	Equivalent modulus Ee	1.13 E + 03
29	Equivalent radius Re	2.3077
30	Ellipse c (mm)	3.41 E + 00
31	Ellipse d (mm)	1.84 E-01
32	Contact pressure, q	4.55 E + 01
33	Ellipse area	1.968
34	Tangential stress	**6.069378005**
35	Tangential stress + Hertz Stress	**20.80**
36	Total shear stress/(ultimate tensile/2)	**0.602861852**
37	Maximum shear stress/(ultimate tensile/2)	0.40
38	Max shear stress	14.73
39		

References

[1] Gogna, A., Peh, W. C. G., and Munk, P. L., 2008, "Image-Guided Musculoskeletal Biopsy," Radiol. Clin. North Am., **46**(3), pp. 455–473.
[2] Pinto, C. H., Taminiau, A. H. M., Vanderschueren, G. M., Hogendoorn, P. C. W., Bloem, J. L., and Obermann, W. R., 2002, "Technical Considerations in CT-Guided Radiofrequency Thermal Ablation of Osteoid Osteoma: Tricks of the Trade," Am. J. Roentgenol., **179**(6), pp. 1633–1642.
[3] Sierre, S., Innocenti, S., Lipsich, J., Lanfranchi, L., Questa, H., and Moguillansky, S., 2006, "Percutaneous Treatment of Osteoid Osteoma by CT-Guided Drilling Resection in Pediatric Patients," Pediatr. Radiol., **36**(2), pp. 115–118.

[4] Ahlstrom, K. H., and Astrom, K. G., 1993, "CT-Guided Bone Biopsy Performed by Means of a Coaxial Biopsy System With an Eccentric Drill," Radiology, **188**(2), pp. 549–552.
[5] Gupta, R., Grasruck, M., Suess, C., Bartling, S., Schmidt, B., Stierstorfer, K., Popescu, S., Brady, T., and Flohr, T., 2006, "Ultra-High Resolution Flat-Panel Volume CT: Fundamental Principles, Design Architecture, and System Characterization," Eur. Radiol., **16**(6), pp. 1191–1205.
[6] Labadie, R., Chodhury, P., Cetinkaya, E., Balachandran, R., Haynes, D., Fenlon, M., Jusczyzck, A., and Fitzpatrick, M., 2005, "Minimally Invasive, Image-Guided, Facial-Recess Approach to the Middle Ear: Demonstration of the Concept of Percutaneous Cochlear Access In Vitro," Otology and Neurotology: official publication of the American Otological Society, American Neurotology Society and European Academy of Otology and Neurotology, **26**(4), pp. 557–562.
[7] Buckley, O., Benfayed, W., Geoghegan, T., Al-Ismail, K., Munk, P. L., and William, C. T., 2007, "CT-Guided Bone Biopsy: Initial Experience With a Commercially Available Hand Held Black and Deckerâ Drill," Eur. J. Radiol., **61**(1), pp. 176–180.
[8] Onogi, S., Morimoto, K., Sakuma, I., Nakajima, Y., Koyama, T., Sugano, N., Tamura, Y., Yonenobu, S., and Momoi, Y., 2005, "Development of the Needle Insertion Robot for Percutaneous Vertebroplasty," MICCAI'05 Proceedings of the 8th International Conference on Medical Image Computing and Computer-Assisted Intervention, Vol. Part II, Springer-Verlag, Berlin/Heidelberg, pp. 105–113.
[9] Majdani, O., Rau, T., Baron, S., Eilers, H., Baier, C., Heimann, B., Ortmaier, T., Bartling, S., Lenarz, T., and Leinung, M., 2009, "A Robot-Guided Minimally Invasive Approach for Cochlear Implant Surgery: Preliminary Results of a Temporal Bone Study," Int. J. Comput. Assisted Radiology and Surgery, **4**(5), pp. 475–486.
[10] Warren, F. M., Balachandran, R., Fitzpatrick, J. M., and Labadie, R. F., 2007, "Percutaneous Cochlear Access Using Bone-Mounted, Customized Drill Guides: Demonstration of Concept In Vitro," Otol. Neurotol., **28**(3), pp. 325–329.
[11] Labadie, R. F., Noble, J. H., Dawant, B. M., Balachandran, R., Majdani, O., and Fitzpatrick, J. M., 2008, "Clinical Validation of Percutaneous Cochlear Implant Surgery: Initial Report," Laryngoscope, **118**(6), pp. 1031–1039.
[12] Chung, G. B., Lee, S. G., Kim, S., Yi,, B.-J., Kim, W.-K., Oh, S. M, Kim, Y.-S., Park, J. I., and Oh, S. H., 2005, "A Robot-Assisted Surgery System for Spinal Fusion," 2005 IEEE/RSJ International Conference on Intelligent Robots and Systems, Edmonton, Alberta, Canada, August 2–6, pp. 3015–3021.
[13] Tsai, T.-C., and Hsu, Y.-L., 2004, "Development of a Parallel Surgical Robot With Automatic Bone Drilling Carriage for Stereotactic Neurosurgery," 2004 IEEE International Conference on Systems, Man and Cybernetics, The Hague, Netherlands, October 10–13, Vol. 3, pp. 2156–2161.
[14] Hsu, Y.-L., Lee, S.-T., and Lin, H.-W., 2001, "A Modular Mechatronic System for Automatic Bone Drilling," Biomed. Eng. Appl. Basis and Communications, **13**(4), pp. 168–174.
[15] Cole, J. D., and Durham, A. G., 1990, "Medical Drill Assembly Transparent to X-Rays and Targeting Drill Bit," U.S. Patent No. 5,013,317.
[16] Hillery, M. T., and Shuaib, I., 1996, *The Drilling of Bone Using Guide Wires and Twist Drills*, M. T. Hillery, ed., Proceedings of the 13th Irish Manufacturing Conference (IMC-13), Limerick, Ireland, September 4–6, pp. 33–42.
[17] Hillery, M. T., and Shuaib, I., 1999, "Temperature Effects in the Drilling of Human and Bovine Bone," J. Mater. Process. Technol., **92**, pp. 302–308.
[18] Lundskog, J., 1972, "Heat and Bone Tissue. An Experimental Investigation of the Thermal Properties of Bone and Threshold Levels for Thermal Injury," Scand. J. Plast. Reconstr. Surg., Suppl. 9, pp. 1–80.
[19] Ohashi, H., Therin, M., Meunier, A., and Christel, P., 1994, "The Effect of Drilling Parameters on Bone," J. Mater. Sci. Mater. Med., **5**(4), pp. 225–231.
[20] Walsh, C., Hanumara, N., Slocum, A., Shepard, J., and Gupta, R., 2008, "A Patient-Mounted, Telerobotic Tool for CT-Guided Percutaneous Interventions," ASME J. Med. Devices, 2(1), p. 011007.
[21] Slocum, A. H., 1992, *Precision Machine Design*, Society of Manufacturing Engineers, Dearborn, MI.
[22] Zivanovic, A., Dibble, E., and Davies, B., 2006, "A High Force Haptic System for Knee Arthroscopy Training," Int. J. Humanoid Robotics (IJHR), **3**(4), pp. 429–437.